Shear flow generation by Reynolds stress and suppression of resistive g modes

H. Sugama
National Institute for Fusion Science, Nagoya 464-01, Japan

W. Horton
Institute for Fusion Studies, The University of Texas at Austin, Austin, Texas 78712

Suppression of resistive g-mode turbulence by background shear flow generated from a small external flow source and amplified by the fluctuation-induced Reynolds stress is demonstrated and analyzed. The model leads to a paradigm for the low-to-high (L–H) confinement mode transition. To demonstrate the L–H transition model, single-helicity nonlinear fluid simulations using the vorticity equation for the electrostatic potential, the pressure fluctuation equation, and the background poloidal flow equation are used in the sheared slab configuration. The relative efficiency of the external flow and the Reynolds stress for producing shear flow depends on the poloidal flow damping parameter ν, which is given by neoclassical theory. For large ν, the external flow is a dominant contribution to the total background poloidal shear flow and its strength predicted by the neoclassical theory is not enough to suppress the turbulence significantly. In contrast, for small ν, it is shown that the fluctuations drive a Reynolds stress that becomes large and suddenly, at some critical point in time, shear flow much larger than the external flow is generated and leads to an abrupt, order unity reduction of the turbulent transport just like that of the L–H transition in tokamak experiments. It is also found that, even in the case of no external flow, the shear flow generation due to the Reynolds stress occurs through the nonlinear interaction of the resistive g modes and reduces the transport. To supplement the numerical solutions, the Landau equation for the mode amplitude of the resistive g mode is derived, taking into account the fluctuation-induced shear flow and the opposite action of the Reynolds stress in the resistive g turbulence compared with the classical shear flow Kelvin–Helmholtz (KH) driven turbulence is analyzed.

I. INTRODUCTION

During recent years, many theoretical works on the relation between plasma turbulence and background shear flow have been done[1–10] in order to understand the physics of the high-mode, which has been experimentally observed in many tokamaks and searched for in other devices, such as stellarators. The reduction of growth rates and saturation levels of many types of instabilities in the presence of background shear flow were theoretically confirmed. However, drawing a closed picture of the H-mode physics requires a description of the mechanism for the generation of the background flow, and several theoretical models for that have been proposed. These models may be classified into two types. One is based on neoclassical or particle orbit loss processes[2,3] and the other is based on turbulent processes or Reynolds stress.[4–6,9,10] The latter yields a simpler picture, in that a self-consistent treatment of the shear flow generation and its turbulence suppression can be constructed within the framework of the fluid model of the plasma dynamics.

In this work, our main concern is in the shear flow generation by the Reynolds stress in the case of the resistive g modes.[11–13] Here the electrostatic fluid model equations are used for the analytical and numerical calculations in the single-helicity sheared slab configurations. It is known that the eigenfunctions of the pure linear resistive g modes yield no Reynolds stress (the word "pure" implies the case that neither background flow nor diamagnetic drift effects are taken into account). Therefore, as a seed of background shear flow, we put an external neoclassical flow velocity into the background momentum balance equation. However, significant suppression of the turbulence is not realized by the external shear flow predicted by neoclassical theory acting alone. It will be shown by the quasilinear analysis and the nonlinear simulations that the Reynolds stress generated by the resistive g modes in the presence of the weak neoclassical shear flow enhances the shear flow generation mechanism, so that the generated shear flow can become much larger than the external neoclassical shear flow, and thus effectively reduce the turbulence level and transport when the collisional flow damping rate is small. This situation is in striking contrast to the case of the Kelvin–Helmholtz (KH) instability,[14,15] where the Reynolds stress weakens the background shear flow. This difference is also characterized by the tilting directions[14] of the vortices in these instabilities, which are opposite to each other. Furthermore, we will find that even in the case that there is no external flow and no diamagnetic drift effect, nonlinear interaction of the pure resistive g modes yields a small seed of background shear flow, which grows up large enough to cause turbulent transport reduction.

This work is organized as follows. In Sec. II, the fluid model equations describing the resistive interchange modes and the background poloidal shear flow are explained. The external shear flow term derived from the neoclassical theory is also described. In Sec. III, we present the quasilinear analysis of the shear flow generation by the Reynolds stress. We find that the eigenfunction of the resistive g mode under the background shear flow yields the Reynolds stress enhancing the flow shear. We also derive the Landau equation for the evolution of the single-mode amplitude of the resistive g mode, taking account of the shear flow generation. In Sec. IV, the shear flow generation and the transport suppression are investigated by the single-helicity nonlinear simulations using the model equations given in Sec. II. Finally, conclusions and a discussion are given in Sec. V.

II. MODEL EQUATIONS

In order to describe the resistive g mode, we use the following equations[12,13] for the electrostatic potential $\phi \equiv \phi_0 + \tilde{\phi}$ and the pressure $p \equiv P_0 + \tilde{p}$ (the subscript 0 denotes the background part and $\sim$ the fluctuation part):

$$\frac{\rho_m c}{B_0} \left(\frac{\partial}{\partial t} - \mu \nabla_\perp^2 + \frac{c}{B_0} \hat{z} \times \nabla \phi \cdot \nabla \right) \nabla_\perp^2 \phi = -\frac{B_0}{c\eta} \nabla_\parallel^2 \phi - \Omega' \frac{\partial \tilde{p}}{\partial y}, \tag{1}$$

$$\left(\frac{\partial}{\partial t} - \chi \nabla_\perp^2 + \frac{c}{B_0} \hat{z} \times \nabla \phi \cdot \nabla \right) \tilde{p} = \frac{c}{B_0} P_0' \frac{\partial \phi}{\partial y}, \tag{2}$$

where B_0 is the component of the static magnetic field along the z axis, ρ_m is the average mass density, c is the light velocity in the vacuum, η is the resistivity, μ is the viscosity, χ is the pressure diffusivity, $P_0' \equiv dP_0/dx$ (<0) is the background pressure gradient, and $\Omega' \equiv d\Omega/dx$ (>0) is the average curvature of the magnetic field line.[16] Here $\nabla_\perp^2 = \partial_x^2 + \partial_y^2$ denotes the two-dimensional Laplacian. The gradient along the static sheared magnetic field line is given by

$$\nabla_\parallel = \frac{\partial}{\partial z} + \frac{x}{L_s} \frac{\partial}{\partial y}. \tag{3}$$

Here B_0, L_s, ρ_m, η, ν, χ, P_0', and Ω' are assumed to be constant, since we treat a local transport problem. The electrostatic approximation is used in Eqs. (1) and (2), since we consider the low beta plasma in the peripheral region.

The dissipation coefficients μ and χ are included to give an energy sink in the high wave number region, which is necessary for the turbulence saturation. We consider that they are dominated by the ion–ion collision and given by the classical or neoclassical expressions.

We employ the following equation for the background poloidal flow $v_E \equiv (c/B_0)(d\phi_0/dx)$:

$$\frac{\partial v_E}{\partial t} + \nu[v_E - V(x)] = -\frac{\partial \langle \tilde{v}_x \tilde{v}_y \rangle}{\partial x}. \tag{4}$$

Here $\tilde{v} = \hat{z} \times \nabla \tilde{\phi}$ and

$$-\langle \tilde{v}_x \tilde{v}_y \rangle \tag{5}$$

represents the Reynolds stress caused by the potential fluctuations, $\langle \cdot \rangle$ is the average in the poloidal y direction, V is the external flow, and ν is the relaxation rate given by the neoclassical theory as[17–19]

$$\nu = \frac{\omega_T q^2 \nu_*}{1 + \nu_*}, \tag{6}$$

$$\omega_T = \frac{v_{T_i}}{qR}, \quad \nu_* = \frac{\nu_i}{\omega_T (r/R)^{3/2}} \tag{7}$$

where v_i denotes the ion thermal velocity, q is the safety factor, and R and r are the plasma major and minor radius, respectively.

Hereafter we use the resistive g units given by

$$[t] = (-P_0' \Omega'/\rho_m)^{-1/2} = \sqrt{L_p L_c}/v_T,$$

$$[x] = [y] = cL_s \eta^{1/2}(-\rho_m P_0' \Omega')^{1/4}/B_0$$
$$= L_s(v_e v_T/\omega_{ce}\omega_{ci}\sqrt{L_p L_c})^{1/2},$$

$$[z] = L_s, \tag{8}$$

$$[\mu] = [\chi] = c[\phi]/B_0$$
$$= [x]^2/[t] = c^2 \eta(-P_0')\Omega' L_s^2/B_0^2$$
$$= D_{cl}(L_s^2/L_p L_c),$$

$$[p] = P_0'[x],$$

where $v_e = n_e e^2 \eta/m_e$ is the electron collision frequency, $D_{cl} = c^2 \eta P_0/B_0^2$ is the classical diffusivity, $\omega_{ce} = eB_0/m_e c$, $\omega_{ci} = eB_0/m_i c$ are the cyclotron frequencies, $v_T = \sqrt{(T_i + T_e)/m_i}$, $L_c = 1/\Omega'$, and $L_p = -P_0/P_0'$. Then we obtain model equations in nondimensional variables from Eqs. (1), (2), and (4) as follows:

$$\partial_t \nabla_\perp^2 \phi + [\phi, \nabla_\perp^2 \phi] = -\nabla_\parallel^2 \phi - \partial_y \tilde{p} + \mu \nabla_\perp^4 \phi, \tag{9}$$

$$\partial_t \tilde{p} + [\phi, \tilde{p}] = -\partial_y \phi + \chi \nabla_\perp^2 \tilde{p}, \tag{10}$$

$$\partial_t v_E + \nu(v_E - V) = -\partial_x \langle \tilde{v}_x \tilde{v}_y \rangle, \tag{11}$$

where

$$v_E \equiv \frac{d\phi_0}{dx},$$

$$\nabla_\parallel = \partial_z + x\partial_y, \tag{12}$$

and

$$[f, g] = (\partial_x f)(\partial_y g) - (\partial_x g)(\partial_y f).$$

III. QUASILINEAR ANALYSIS

We now consider a linear mode of the form $\tilde{\phi} = \phi_k(x)e^{iky - i\omega t}$ under the background shear flow $v_E(x)$, with the mode resonant surface of which is located at $x = 0$. Linearization of Eqs. (1) and (2) yields the following mode equation:

H. Sugama and W. Horton

$$\left(\frac{d^2}{dx^2}-k^2+\underbrace{\frac{kv_E''}{\omega-kv_E}}_{\text{KH}}-\underbrace{\frac{k^2}{(\omega-kv_E)^2}}_{g\text{ mode}}-\underbrace{\frac{ik^2x^2}{\omega-kv_E}}_{\text{magnetic shear}}\right)\phi_k(x)=0,$$

(13)

where the viscosity μ and pressure diffusivity χ were neglected and the last three terms on the left-hand side correspond to Kelvin–Helmholtz (KH), g mode, and magnetic shear effects, respectively. Contribution from the mode $\phi_k(x)=|\phi_k(x)|\exp[i\theta_k(x)]$ to the poloidal acceleration due to quasilinear Reynolds stress is given by

$$-\frac{\partial\langle\tilde{v}_x\tilde{v}_y\rangle}{\partial x}=ik\frac{d}{dx}\left(\phi_k\frac{d\phi_k^*}{dx}-\phi_k^*\frac{d\phi_k}{dx}\right)$$

$$=2k\frac{d}{dx}\left(|\phi_k|^2\frac{d\theta_k}{dx}\right)=2|\phi_k|^2\left[\omega_i\left\{\underbrace{\frac{k^2v_E''}{|\omega-kv_E|^2}}_{\text{KH}}+\underbrace{\frac{2k^4v_E}{|\omega-kv_E|^4}\left(1-\frac{\omega_r}{kv_E}\right)}_{g\text{ mode}}\right\}-\underbrace{\frac{k^4x^2v_E}{|\omega-kv_E|^2}\left(1-\frac{\omega_r}{kv_E}\right)}_{\text{magnetic shear}}\right],$$

(14)

where we used Eq. (13) and $\omega=\omega_r+i\omega_i$. If we assume that the background poloidal shear flow $v_E(x)$ has the profile in the form of $v_E(x)=v_0\tanh(x/L_E)$, or $v_E(x)=v_0\sin(x/L_E)$, we find that the sign of $v_E''\equiv d^2v_E/dx^2$ is opposite to that of v_E and that we can put $\omega_r=0$ and $\theta_k(-x)=-\theta_k(x)$. Then it can be seen from Eq. (14) that, for the unstable mode $\omega_i>0$, the KH and magnetic shear terms weaken the shear flow while the g-mode term strengthens it.

Characterizing the general shear flow profile $v_E(x)$ in terms of its maximum value v_0 and characteristic length L_E, the ratio of the g-mode term to the KH term in Eq. (14) is estimated as $2k^2[v_E/v_E''](\gamma^2+k^2v_E^2)^{-1}\simeq(2G/(1+G))(L_E/\Delta)^2$, where Δ denotes the radial mode width and $G\equiv(L_E/v_0)^2(v_T^2/L_pL_c)$. In making this estimate, we use that for low wave numbers the resistive g growth rate γ and mode width Δ are related by $\gamma/k^2\Delta\sim1$ in our units (8). From Ref. 7, $G>1$ is required for the unstable resistive g mode. Considering the typical case where $\Delta<L_E$, we find that the contribution of the g-mode term to the shear flow generation overcomes the damping due to KH term in the g-mode unstable case. As the shear flow grows, the magnitude of G decreases. Then the relative contribution from the g-mode term also decreases, and the fluctuations are more stabilized so that the Reynolds stress effect is weakened. Thus the shear flow generation by the Reynolds stress is considered to work more effectively in the low to high (L–H) transition phase than in the H-mode phase. When the shear flow becomes extremely large, the KH term is the dominant contribution, and the KH instability appears instead of the resistive g mode. However, the criterion for the KH instability[7,13] is not satisfied in the practical experimental parameters, and this KH unstable case is not considered in the simulations in the next section.

For simplicity, let us consider the potential eigenfunction of the form

$$\phi_k(x)=|\phi_k(x)|\exp(ik\alpha x),$$

(15)

where α represents a tilting angle of the vortex with respect to the poloidal direction. In this case, we have

$$-\frac{\partial\langle\tilde{v}_x\tilde{v}_y\rangle}{\partial x}=2k^2\alpha\frac{d|\phi_k(x)|^2}{dx}.$$

(16)

Figures 1(a) and 1(b) show the contours of the potential eigenfunctions given by Eq. (15) with different signs of tilting angles α. Since generally $xd|\phi_k(x)|^2/dx$ is negative, Eq. (16) shows that the background shear flow is decreased by the Reynolds stress for $\alpha v_E'>0$ [Fig. 1(a)] but increased for $\alpha v_E'<0$ [Fig. 1(b)]. For the pure KH instability, it was confirmed in Ref. 14 that the vortex tilting satisfied the condition $\alpha v_E'>0$ and weakened the shear flow, which agrees with the our present prediction based on Eq. (14). On the other hand, for the resistive g mode under the background shear flow, we will verify later by simula-
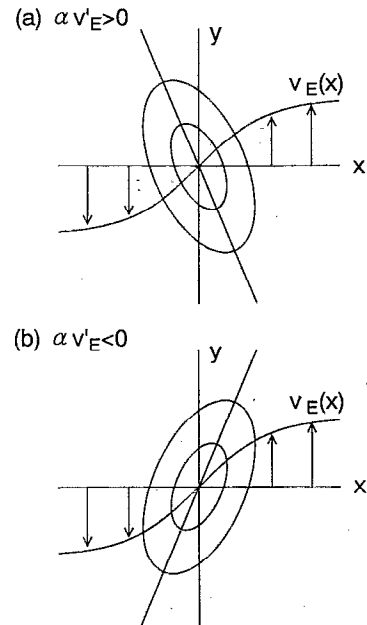

FIG. 1. The contours of potential eigenfunctions given by Eq. (15). The quasilinear Reynolds stress increases the shear of the background poloidal flow for (a) $\alpha v_E'>0$ and decreases it for $\alpha v_E'<0$.

tions that the direction of the vortex tilting is opposite to that of the pure KH instability, and the shear flow is enhanced by the Reynolds stress.

Next, we treat the resistive g mode under the background poloidal shear flow near the marginally stable state by the weakly nonlinear theory.[20–22] Here, we assume that the system is weakly unstable and that the maximum linear growth rate is slightly larger than zero. In such a weakly unstable state, fluctuation amplitudes and their temporal variation are small, and their smallness are represented by the parameter λ. We make the following perturbation expansion with the parameter λ:

$$\begin{pmatrix} \widetilde{\phi} \\ \widetilde{p} \end{pmatrix} = \lambda \begin{pmatrix} \widetilde{\phi}_1 \\ \widetilde{p}_1 \end{pmatrix} + \lambda^2 \begin{pmatrix} \widetilde{\phi}_2 \\ \widetilde{p}_2 \end{pmatrix} + \cdots,$$

$$\frac{\partial}{\partial t} = \lambda \frac{\partial}{\partial \tau_1} + \lambda^2 \frac{\partial}{\partial \tau_2} + \cdots, \qquad (17)$$

$$v_E = v_{E0} + \lambda v_{E1} + \lambda^2 v_{E2} + \cdots .$$

Since λ is only the formal expansion parameter, we can put $\lambda = 1$ in the final results, or, in other words, λ can be included into the fluctuation amplitudes and time derivatives themselves. We put the external poloidal flow $V(x)$ as

$$V = V_c + \lambda^2 V_2. \qquad (18)$$

In the marginally stable state $\lambda = 0$, Eqs. (11) and (18) give the background poloidal flow $v_E = V_c$, for which the maximum growth rate of the mode with the lowest wave number k is zero. It should be noted that the marginal stability requires finite values for μ and χ. For $\lambda \neq 0$, the system becomes linearly unstable, since we assume that V_2 in the external flow weakens the shear of V_c and lowers its stabilizing effect.

In $O(\lambda)$, Eqs. (9) and (10) yield the linear eigenmode equations, the solution of which is written as

$$\begin{pmatrix} \widetilde{\phi}_1 \\ \widetilde{p}_1 \end{pmatrix} = A e^{iky} \begin{pmatrix} \phi_1(x) \\ p_1(x) \end{pmatrix} + A^* e^{-iky} \begin{pmatrix} \phi_1^*(x) \\ p_1^*(x) \end{pmatrix}, \qquad (19)$$

where we considered the mode with the resonant surface at $x = 0$ only. Here $\phi_1(x)$ and $p_1(x)$ are the eigenfunctions obtained from the $O(\lambda)$ equations, although we need to proceed to higher-order equations to determine the amplitude A.

In the $O(\lambda^2)$ equations, the beating of the first-order fluctuations $\widetilde{\phi}_1$ and $\widetilde{p}_1$ produces the second-order fluctuations, which have the poloidal wave numbers 0 and $2k$. From the solvability condition of the $O(\lambda^2)$ equations for the wave number k, we have

$$\partial_{\tau_1} A = 0. \qquad (20)$$

Hereafter, in the $O(\lambda^2)$ perturbations, we neglect the effects of the fluctuations with the poloidal wave number $2k$,

and take account of only the background pressure and poloidal flow modifications, which correspond to the poloidal wave number 0. These background corrections are the dominant $O(\lambda^2)$ effects in the cases presented here, and are derived from Eqs. (10) and (11) as

$$p_2' = \frac{2k}{\chi} |A|^2 \text{Imag}(p_1^* \phi_1) \equiv |A|^2 p_{QL}', \qquad (21)$$

$$v_{E2} = V_2 + \frac{2k}{\nu} |A|^2 \text{Imag}[\partial_x(\phi_1^* \partial_x \phi_1)]$$

$$\equiv V_2 + |A|^2 v_{QL}, \qquad (22)$$

where $|A|^2 p_{QL}'$ denotes the quasilinear correction for the background pressure gradient, V_2 is the deviation of the external flow from its critical profile, which gives the linear instability, and $|A|^2 v_{QL}$ represents the background poloidal flow generated nonlinearly (or quasilinearly) by the Reynolds stress due to the first-order potential fluctuations.

We now obtain the following Landau equation from the solvability condition of the $O(\lambda^3)$ equations from the secular variation at the wave number k:

$$\partial_t A = (-i\omega - D|A|^2)A. \qquad (23)$$

Here $\omega = \omega_r + i\omega_i$ is the linear eigenfrequency and $D = D_r + iD_i$ is the complex-valued constant determined by the shape and phase of the eigenmode. The third-order solvability condition gives the formulas

$$-i\omega = D_1/D_0,$$

$$D = D_3/D_0,$$

where

$$D_0 = \int dx(\phi_1^\dagger(-\partial_x^2 + k^2)\phi_1 - p_1^\dagger p_1),$$

$$D_1 = -ik \int dx\{V_2[\phi_1^\dagger(-\partial_x^2 + k^2)\phi_1 - p_1^\dagger p_1]$$

$$+ V_2'' \phi_1^\dagger \phi_1\}, \qquad (24)$$

$$D_3 = ik \int dx\{v_{QL}[\phi_1^\dagger(-\partial_x^2 + k^2)\phi_1 - p_1^\dagger p_1]$$

$$+ v_{QL}'' \phi_1^\dagger \phi_1 + p_{QL}' p_1^\dagger \phi_1\},$$

where $\phi_1^\dagger$ and $p_1^\dagger$ are the eigenfunctions determined by the linear equations adjoint to those for ϕ_1 and p_1. The Landau equation (23) is analytically solved for the growth and saturation of the single-mode amplitude given by

$$|A(t)|^2 = \frac{|A(0)|^2}{(D_r/2\omega_i)|A(0)|^2 + [1 - (D_r/2\omega_i)|A(0)|^2]\exp(-2\omega_i t)}. \qquad (25)$$

H. Sugama and W. Horton

Generally the quasilinear pressure flattening represented by p'_{QL} contributes to the saturation of the amplitude, and we will see later that the flow generated by the Reynolds stress v_{QL} also causes the amplitude saturation in both cases of the pure KH instability and the resistive g mode under the background poloidal shear flow. The saturation amplitude and the convective transport are given by

$$|A|^2 = \frac{2\omega_i}{D_r}, \qquad (26)$$

$$\langle \tilde{p}\,\tilde{v}_x \rangle = 2k|A|^2 \, \mathrm{Imag}(p_1^* \phi_1). \qquad (27)$$

If we assume that $v_E(-x) = -v_E(x)$, we have a pure imaginary linear eigenfrequency $\omega = i\omega_i$ and a complex-valued eigenfunction $\phi_1(x)$, satisfying $|\phi_1(-x)| = |\phi_1(x)|$ and $\arg \phi_1(-x) = -\arg \phi_1(x)$. Then D_0, D_1, and D_3 are all real-valued constants. For linear instability, the deviation V_2 of the external poloidal flow from that in the marginal stable state is required to increase the shear for the pure KH instability case and decrease it for the resistive g-mode case. As we found previously in this section, the Reynolds-stress-produced flow v_{QL} works opposite to V_2. Then, comparing the contribution of V_2 to D_1 with that of v_{QL} to D_3 in Eq. (24), we see that D_1 and D_3 (or ω_i and D) have the same sign. Thus D is positive and v_{QL} contributes to the amplitude saturation in both the KH and the resistive g-mode cases. From Eqs. (22) and (24), v_{QL} and D_3 are inversely proportional to ν so that the saturation amplitude (26) and the transport flux (27) are lowered for smaller values of ν.

Analytical treatments in this section are quantitatively accurate in the system near the marginally stable state while they give only qualitative suggestions for the behavior in the strongly nonlinear or turbulent state, in which it is difficult to apply analytical methods and a numerical solution as in Sec. IV is required. Here we emphasize the analytically predicted tendencies that, under the background shear flow, the Reynolds stress due to the resistive g mode enhances the shear, in contrast with the KH case, and that larger shear flow generation and smaller saturated transport are obtained for smaller values of ν.

IV. SIMULATION RESULTS

Equations (9)–(11) are numerically solved in the sheared slab configuration. Here we concentrate on the single-helicity (or two-dimensional) nonlinear simulations, in which all the Fourier modes of fluctuations are assumed to have the same mode resonant surface at $x=0$. We put the boundaries at $x = \pm a$, which are chosen such that the fluctuations are damped enough by the magnetic shear before reaching the boundaries. We use the external poloidal flow profile in the form of

$$V(x) = V_0 \sin(\pi x / 2a), \qquad (28)$$

which gives the vorticity as

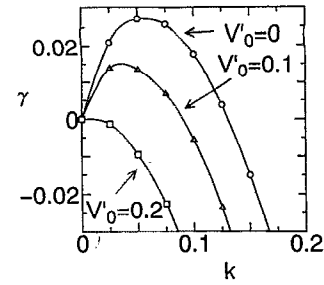$$V'(x) = V_0' \cos(\pi x / 2a) \qquad (29)$$

FIG. 2. The linear growth rates for the resistive g mode under the background poloidal flow given by the external one [Eq. (28)]. Three curves corresponds to different values of the maximum vorticity (or shear) V_0': $V_0' = 0$ (no background flow case), $V_0' = 0.1$, and $V_0' = 0.2$.

where $V_0' = \pi V_0 / 2a$ gives the maximum vorticity (or shear). We employ the boundary conditions given by

$$\tilde{\phi} = \partial_x^2 \tilde{\phi} = \tilde{p} = 0, \quad \text{at } x = \pm a. \qquad (30)$$

As initial conditions of the simulations, we give perturbations to all the single-helicity modes in the form of the linear eigenfunctions with the same kinetic energy and the random phase relation to each other. Since our concerns in this study are with the background shear flow production due to the Reynolds stress, we neglect the quasilinear pressure flattening and fix the background pressure gradient, which is equivalent to the addition of a certain source term to the pressure equation. In all the simulations here, the normalized viscosity and pressure diffusivity are given by $\mu = \chi = 4.0$. In the dimensional form, they are written as $\mu = \chi = 4.0 D_{cl} L_s^2 / L_p L_c$, which corresponds to the order of the ion classical diffusivity, since typically we have $L_s^2 / L_p L_c \sim 10$. (When we employ the classical ion viscosity and thermal diffusivity, the nondimensional parameters μ and χ normalized by $[x]^2 / [t] = D_{cl} L_s^2 / L_p L_c$ are independent of plasma density and temperature, but only depending on the ratio T_e / T_i and the geometrical factor $L_s^2 / L_p L_c$.) The potential and pressure fluctuations are Fourier expanded as

$$\begin{pmatrix} \tilde{\phi} \\ \tilde{p} \end{pmatrix} = \sum_m \begin{pmatrix} \phi_m(x,t) \\ p_m(x,t) \end{pmatrix} \exp(imky), \qquad (31)$$

where $k \equiv 2\pi / L_y$ is the minimum poloidal wave number and we use $k = \frac{1}{40}$ in the simulations. From Eq. (8), the unit length $[y]$ depends on the plasma density and temperature, etc. and typically $[y]/\rho_i \approx 0.1$–1.0 (ρ_i is the ion thermal Larmor radius). Then the maximum poloidal wavelength L_y used here corresponds to 10–100 times larger than ρ_i.

Figure 2 shows the linear growth rates for the resistive g mode under the background poloidal flow given by the external one [Eq. (28)]. When the background poloidal flow has the maximum shear $V_0' = 0.2$, the system is completely linear stable.

The nonlinear time evolution of the kinetic energy and the convective transport are shown in Figs. 3 and 4. There the same external shear flow with $V_0' = 0.1$ is used and the same initial perturbation is given to the $m=1$ mode potential. The only difference in the parameters for Figs. 3 and 4
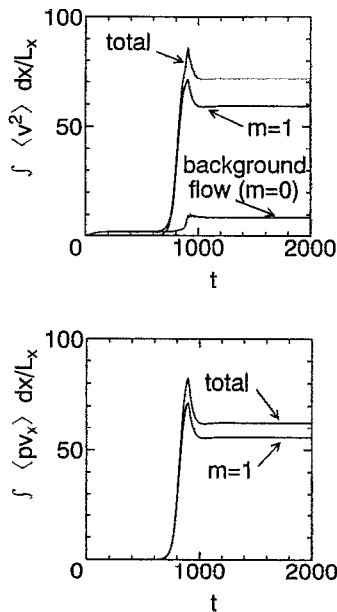
FIG. 3. The time evolution of the kinetic energy $\frac{1}{2}\int dx\langle v^2\rangle$ and the convective transport $\int dx\langle \tilde{p}\,\tilde{v}_x\rangle$ for $V_0' = 0.1$ and $\nu = 0.02$.

is the values of the relaxation rate ν in the momentum balance Eq. (11): $\nu = 0.02$ in Fig. 3 and $\nu = 0.3$ in Fig. 4. In both figures, we can see that the $m = 1$ mode, which is the most unstable mode with the minimum poloidal wave number, gives the dominant contribution to the kinetic energy and the transport in the nonlinearly saturated states. The most remarkable feature of the comparison is that, in the small ν case of Fig. 3, a strong background ($m = 0$) poloidal flow is generated and that this flow
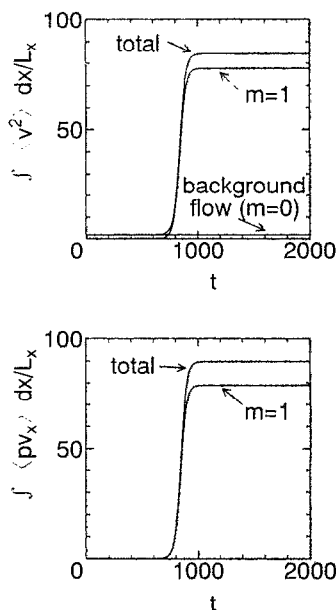

FIG. 4. The time evolution of the kinetic energy $\frac{1}{2}\int dx\langle v^2\rangle$ and the convective transport $\int dx\langle \tilde{p}\,\tilde{v}_x\rangle$ for $V_0' = 0.1$ and $\nu = 0.3$.
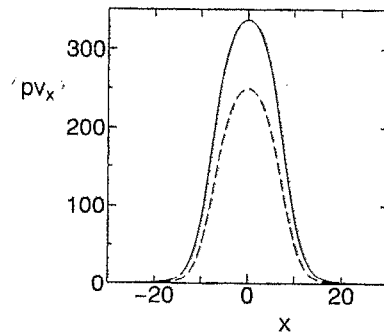

FIG. 5. Radial profiles of the convective flux $\langle \tilde{p}\,\tilde{v}_x\rangle$ in the cases of Figs. 3 (a dashed line) and 4 (a solid line).

strongly reduces the fluctuation kinetic energy and the associated radial thermal transport. On the other hand, in the large ν case of Fig. 4, neither generation of a significant background flow, nor the reduction of the fluctuation kinetic energy and the transport occur. These results are qualitatively consistent with those of the quasilinear analysis in the previous section, where it was shown that the Reynolds-stress-produced flow increases and the saturation amplitude decreases as ν becomes smaller. The temporal evolution described by Eq. (25) qualitatively agrees with the numerical results in Figs. 3 and 4, in that Eq. (25) shows the saturation of the dominant $m = 1$ mode as well as its linear growth, although it fails to describe the overshooting observed in Fig. 3, which may be due to highly nonlinear effects.

Figure 5 shows radial profiles of the convective flux $\langle \tilde{p}\,\tilde{v}_x\rangle$ in the cases of Figs. 3 and 4. Both profiles are of the Gaussian form with the same radial width. The radial structures of the $m = 1$ mode potential and pressure in these cases are almost the same as those of the linear eigenfunctions. The flux amplitude for $\nu = 0.02$ is about three-fourths of that for $\nu = 0.3$.

Figure 6 shows radial profiles of the background poloidal flow $v_E(x)$ and the vorticity $v_E'(x)$ at the time $t = 2000$ in the case of Fig. 3. There profiles of the external flow $V(x)$ and vorticity $V'(x)$ are also plotted by the dashed lines. It is seen that the maximum shear (or vorticity) of the background flow generated by the Reynolds stress is about six times larger than that of the external flow. At this shear of the background flow, linear perturbation theory gives the completely stabilized state with no fluctuations. However, the saturated or quasisteady state with finite amplitude of fluctuations is obtained in the simulation of Fig. 3.

The contours of the $m = 1$ mode of the electrostatic potential in the case of Fig. 3 are shown in Fig. 7. There (a) is for the growing state ($t = 500$) and (b) for the saturated state ($t = 2000$). It is found that the vortex tilts in the same direction as in Fig. 1(b), which implies the Reynolds stress enhancing the shear of the background poloidal flow. The vortex tilting is clearer in (a) than in (b). In case (a) the shear flow generation due to the Reynolds stress exceeds the collisional damping (denoted by ν),
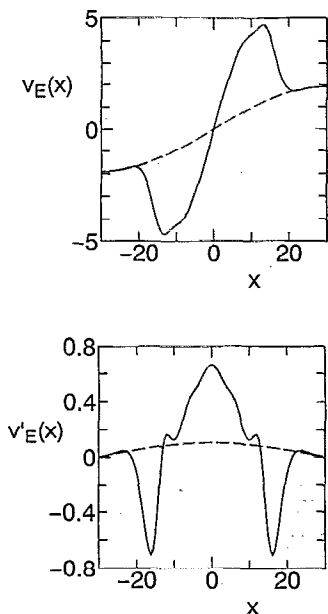
H. Sugama and W. Horton

FIG. 6. Radial profiles of the background poloidal flow $v_E(x)$ and the vorticity $v'_E(x)$ at the time $t=2000$ in the case of Fig. 3. The dashed lines denote the external flow $V(x)$ and vorticity $V'(x)$.

while in the case (b) they are balanced with each other. In the saturated state (b), the fluctuation amplitude is high, and therefore only a small tilting angle is required to maintain the shear flow if v is small.
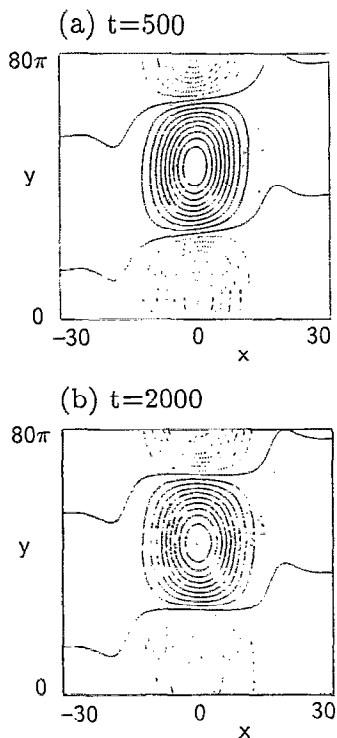

FIG. 7. The contours of the $m=1$ mode of the electrostatic potential in the case of Fig. 3. Here (a) is for the growing state ($t=500$) and (b) is for the saturated state ($t=2000$).
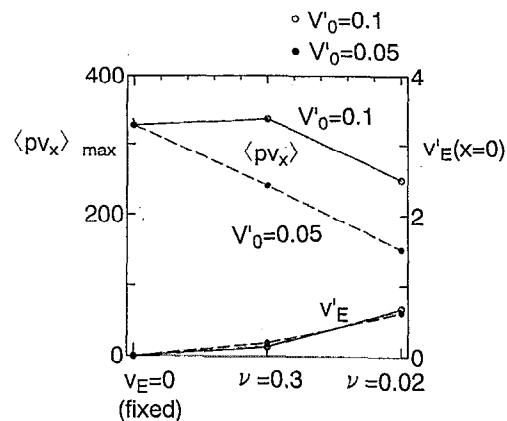

FIG. 8. The convective flux $\langle \tilde{p}\,\tilde{v}_x \rangle$ and the background poloidal flow v'_E at the mode resonant surface $x=0$ for $v=0.02$ and $v=0.3$. The solid circles correspond to the case of $V'_0 = 0.05$, and the open circles to the case of $V'_0 = 0.1$. Also plotted is the convective transport, in the case where the background flow is fixed to be zero. The dominant mode number in the saturated state is $m=2$ for no background flow and $V'_0 = 0.05$ cases, and $m=1$ for $V'_0 = 0.1$.

Figure 8 shows the convective flux $\langle \tilde{p}\,\tilde{v}_x \rangle$ and the background poloidal flow shear v'_E at the mode resonant surface $x=0$ for $v=0.02$ and $v=0.3$. The solid circles correspond to the case of $V'_0 = 0.05$ and the open circles to the case of $V'_0 = 0.1$. Also plotted is the convective flux in the case where the background flow is fixed to be zero. For smaller v, the Reynolds stress generates a higher shear in the background shear flow, and thus a larger reduction of the transport. In the case of no background flow and $V'_0 = 0.05$, the dominant poloidal mode number in the saturated state is $m=2$, which corresponds to the most linearly unstable mode. On the other hand, for $V'_0 = 0.1$, the $m=1$ mode, which has the maximum linear growth rate, becomes dominant in the saturated state and gives larger transport than in the $m=2$ mode dominant case. In the saturated states, we always found that only one mode is dominant, and contributions from the other modes to the energy and transport are much smaller than the dominant mode contribution. (We never observed the cases in which both the $m=1$ and $m=2$ modes had comparable amplitudes.) It seems that the mode that has grown faster suppresses the other modes.

In Fig. 9, the convective flux, the background poloidal flow shear at $x=0$, and the maximum linear growth rate are shown for different values of V'_0. Here $v=0.02$ is used. The dominant poloidal mode number in the saturated state is $m=2$ for $V'_0 = 0, 0.02, 0.05$, and $m=1$ for $V'_0 = 0.1$. In the $m=2$ mode dominant cases, the convective flux gradually decreases as V'_0 increases. However, in the $m=1$ mode dominant case, larger transport is found again in spite of the smaller linear growth rate and the larger Reynolds-stress-produced background vorticity. Generally, nonlinear saturation levels of modes with smaller wave numbers tend to be less affected by the reduction of the linear growth rates and give larger transport.

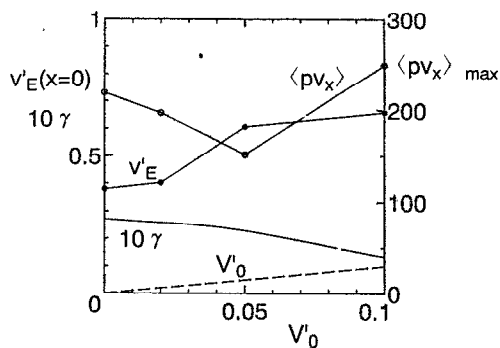As seen from Fig. 3, any fluctuation with small ampli-

FIG. 9. The convective flux, the background poloidal flow shear at $x=0$ and the maximum linear growth rate γ for of $V_0' = 0$, 0.02, 0.05, and 0.1. Here $\nu=0.02$. The dominant poloidal mode number in the saturated state is $m=2$ for $V_0' = 0$, 0.02, 0.05, and $m=1$ for $V_0' = 0.1$.

tude damps in the course of time for $V_0' > 0.2$. Figures 10–12 show the time evolution of the kinetic energy and the turbulent transport for two cases in which the external parameters are changed halfway through the time interval. In Figs. 10 and 11, we put $v_E=0$ for $0 < t < 1000$, and then subsequently v_E is given by solving Eq. (11) with $V_0' = 0.4$ for $t > 1000$. Here $\nu=0.3$ is used in Fig. 10 and $\nu=0.02$ in Fig. 11. In the large ν case (Fig. 10), the background flow v_E approaches to the external one V_0 immediately after $t=1000$. Then the fluctuation energy decreases and the transport is reduced to less than one-seventh of that in the no shear flow case ($t < 1000$). We should note that the value of the maximum background vorticity $V_0' = 0.4$, causing the significant reduction of the turbulent transport, is about twice that required for the linear marginal stability of the system (see Fig. 2), although the transport is not reduced
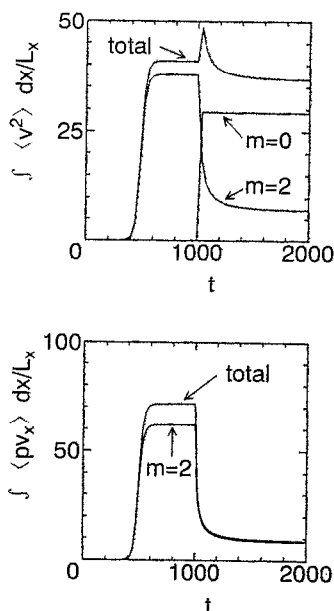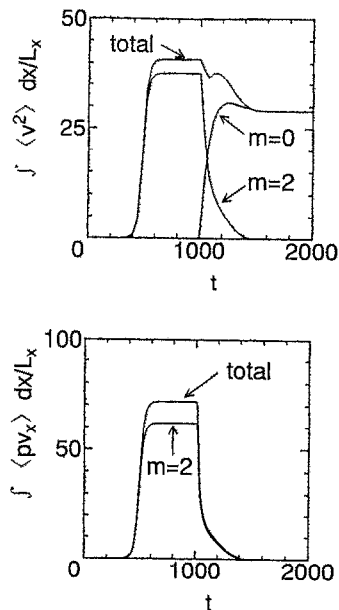

FIG. 11. The time evolution of the kinetic energy and the turbulent transport. Here $v_E=0$ for $0 < t < 1000$, and v_E is given by solving Eq. (11) with $V_0' = 0.4$ and $\nu=0.02$ for $t > 1000$.

in the external flow with $V_0' = 0.1$ (see the case of $V_0' = 0.1$ and $\nu=0.3$ in Fig. 8), for which the linear growth rates is considerably decreased. (We already found the large background vorticity $\simeq 0.7$ in Fig. 6, where the decrease of the transport was also observed.) Thus, in the nonlinear turbulent regime, significant transport reduction can be realized only when the background flow has a shear that is much higher than that predicted by the linear sta-
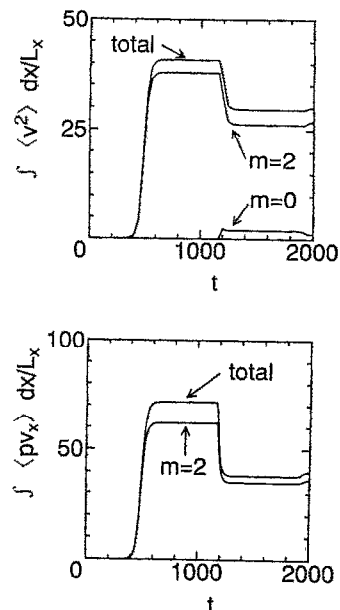

FIG. 10. The time evolution of the kinetic energy and the turbulent transport. Here $v_E=0$ for $0 < t < 1000$, and v_E is given by solving Eq. (11) with $V_0' = 0.4$ and $\nu=0.3$ for $t > 1000$.

FIG. 12. The time evolution of the kinetic energy and the turbulent transport. Here $v_E=0$ for $0 < t < 1000$, and v_E is given by solving Eq. (11) with no external flow ($V_0=0.0$) and $\nu=0.02$ for $t > 1000$.

H. Sugama and W. Horton

bility criterion. In the small ν case (Fig. 11), the Reynolds stress enables the background shear flow to exceed the external flow after $t=1000$, which leads to the complete suppression of the fluctuations and no turbulent transport.

In Fig. 12, no external flow ($V_0=0.0$) is given for $t>1000$, while ν is the same as in Fig. 11 ($\nu=0.02$). In this case, we also find that the Reynolds stress effectively produces the background flow, which reduces the fluctuation level and the transport. The shear flow generation and the transport reduction occur at $t\sim1200$, with some delay after the change of the simulation conditions. The vortex tilting required for the nonvanishing Reynolds stress in this case is produced, not by the external shear flow V_0, but by the nonlinear interactions of the modes with different wave numbers. This interaction process will be discussed in the next section. Interestingly, a small decrease in the background shear flow accompanied with an increase of the fluctuation and the transport is observed suddenly at $t\sim1900$, when no external change of the plasma conditions (like that at $t=1000$) is introduced.

Up to this point, we fixed the values of μ, χ, and $k=2\pi/L_y$. The numerical results can be influenced by these dissipation coefficients as well as the maximum poloidal wavelength L_y. These parameters determine the number of the modes that need to be included in the simulations for obtaining the nonlinearly saturated states. Simulations using different values for these parameters were also done, and we found that, for larger L_y with fixed μ and χ (or for smaller μ and χ with fixed L_y), behavior of fluctuations becomes more turbulent, and the high wave number Reynolds stress contribution to the flow damping increases in the steady turbulence phase, although the shear flow generation by the Reynolds stress still appears in the transition phase.

The change of ν in Figs. 10–12 models the temperature increase due to the thermal flux into the peripheral region accompanied by the auxiliary heating or the sawtooth phenomena. Since it is observed that these thermal influx phenomena trigger the L–H transition, our results seem to be consistent with the experiments. Since the damping coefficient ν as well as the energy input to the fluctuation are dependent on background plasma parameters such as pressure, temperature, and their gradients, we should also take into account the reaction of the background parameters from the influence of the plasma turbulence, which has been disregarded here. A self-consistent treatment of mixed mechanisms of the background response, change in ν, fluctuations, and shear flow is required for a more complete description of the L–H transition and remains for a future problem.

V. CONCLUSIONS AND DISCUSSION

In this work, we investigate the generation of shear flow by the Reynolds stress arising from self-consistent pressure gradient-driven fluctuations, and the resultant reduction of the turbulent transport in the case of the resistive g modes. As found in Eqs. (14) or (16), the radial variation of the phase of the fluctuation, or the vortex tilting is required to yield the nonvanishing Reynolds stress.

In Ref. 5, Diamond *et al.* also argued that the flow generation by the Reynolds stress requires a radial asymmetry in the turbulence spectrum, which corresponds to the radial phase variation or to the vortex tilting. (As in the case of the KH instability, some fluctuations with radially asymmetric mode structures yield the Reynolds stress, which acts as an anomalous viscosity and damps the background shear flow.) Accordingly, they argued that the pure resistive g mode, which has a symmetry in the radial mode structure, gives no Reynolds stress and no background shear flow. However, the radial asymmetry or phase variation appears in the modes under the effect of a small background shear flow, as seen in Sec. III, or it is also spontaneously generated by the nonlinear interaction of pure resistive g modes with different phases, yielding a seed for the flow generation that is shown in Fig. 12. The property of the radial symmetry in the resistive g mode is reflected by the fact that both signs of the shear are realized with with equal probability. Thus, the result in Fig. 12 shows a typical example of a spontaneous broken symmetry and gives the physically important new point of view to understanding the L–H transition. Shear flow effects were also investigated by Carreras *et al.*[4,9,10] in the cases where the shear flow is given initially or by diamagnetic effects. The shear flow generation due to the nonlinear interaction of the resistive g modes in the case of no external and no diamagnetic flow, and the important role of the collisional flow damping parameter ν in the L–H transition were first pointed out in our work.

The production of the phase variation by the nonlinear interaction is described as follows. For example, let us consider linear modes $m=2$, 3, 4, which have constant but different phases. Such a situation is possible, even in the pure g-mode case. Nonlinear interactions of the $m=2$ and $m=3$ modes and that of the $m=3$ and $m=4$ modes both contribute to the production of the $m=1$ mode. If we represent the contributions of these nonlinear interactions to the $m=1$ mode by $\phi_a(x)=|\phi_a(x)|e^{i\theta_a}$ and $\phi_b(x)=|\phi_b(x)|e^{i\theta_b}$, the phases θ_a and θ_b are constants. However, the sum of them $|\phi_a(x)|e^{i\theta_a}+|\phi_b(x)|e^{i\theta_b}=||\phi_a(x)|e^{i\theta_a}+|\phi_b(x)|e^{i\theta_b}|e^{i\theta(x)}$ has a x-dependent phase $\theta(x)$ since $|\phi_a(x)|$ and $|\phi_b(x)|$ generally have different profiles. Thus the nonlinearly produced $m=1$ mode has a radially varying phase and yields the nonvanishing Reynolds stress, which, in turn, causes the background shear flow.

Once the background shear flow is generated, the radial dependence of the mode phase appears, even through the linear process. In Sec. III, we found that the resistive g mode in the background shear flow has a phase variation or vortex tilting that enhances the shear flow, which is in sharp contrast to the pure KH instability case. In the KH case, the shear flow is weakened by vortex tilting. However, as found in Sec. III and Sec. IV, both the KH instability and the resistive g mode arranges the shear flow such that their growth rates are reduced, and therefore the system approaches the stationary state. It is instructive to consider these mechanisms from the point of view based on the energetics. Neglecting all the dissipation terms in Eqs.

(9)–(11), we obtain the following energy conservation law:

$$\frac{d}{dt} \int_{-a}^{+a} dx \left(\frac{1}{2} v_E^2 + \frac{1}{2} \langle \tilde{v}^2 \rangle - xP_0 \right) = 0, \qquad (32)$$

where the contributions from the boundary surfaces are assumed to vanish. Here the first term on the left-hand side is the kinetic energy of the background flow, the second term is the turbulent kinetic energy, and the last term is the released plasma internal energy. In the reference frame where the volume-averaged flow velocity $(1/2a) \int_{-a}^{+a} dx\, v_E(x)$ vanishes, as seen in Sec. IV, the background kinetic energy $\frac{1}{2} \int dx\, v_E^2$ is also a measure of the flow shear or the vorticity. The transfer rates between the three energy components of the energy balance equation are given by

$$\frac{d}{dt} \int dx \frac{1}{2} v_E^2 = -\int dx\, v_E \frac{\partial \langle \tilde{v}_x \tilde{v}_y \rangle}{\partial x}, \qquad (33)$$

$$\frac{d}{dt} \int dx \frac{1}{2} \tilde{v}^2 = \int dx \left(v_E \frac{\partial \langle \tilde{v}_x \tilde{v}_y \rangle}{\partial x} + \langle \tilde{p}\, \tilde{v}_x \rangle \right), \qquad (34)$$

$$\frac{d}{dt} \int dx(-xP_0) = -\int dx \langle \tilde{p}\, \tilde{v}_x \rangle. \qquad (35)$$

In the pure KH instability case, where the pressure gradient terms are not taken into account, the turbulent kinetic energy is supplied by the background shear flow in the growing phase of the instability, and therefore we find from the above equations that $-\partial \langle \tilde{v}_x \tilde{v}_y \rangle / \partial x$ has the opposite sign of v_E, i.e., the Reynolds stress reduces the background shear flow at the rate given by Eq. (33). On the other hand, in the resistive g-mode case, the turbulent energy comes from the plasma internal energy (or the background pressure gradient) in the form of the flux $\langle \tilde{p}\, \tilde{v}_x \rangle$. In this case, the background shear flow weakens the growth of the mode, so the term $\int dx\, v_E(\partial \langle \tilde{v}_x \tilde{v}_y \rangle / \partial x)$ $= -\int dx \langle \tilde{v}_x \tilde{v}_y \rangle\,(\partial v_E / \partial x)$ is negative, which implies that $-\partial \langle \tilde{v}_x \tilde{v}_y \rangle / \partial x$ has the same sign as v_E, i.e., the Reynolds stress enhances the background shear flow.

In Ref. 6, Drake et al. showed the spontaneous generation of the background flow resulting from a certain kind of instability in the neutral fluid, while, in our work, the spontaneous generation is shown, as discussed in Eqs. (33)–(35), from the energy stored originally in the plasma with the pressure gradient and the unfavorable magnetic curvature. The thermal energy is finally converted to the shear flow kinetic energy by way of the resistive g-mode fluctuations.

In conclusion, we have shown in some detail how the Reynolds stress driven by the self-consistent plasma fluctuations works effectively for the generation of a shear flow that reduces the thermal transport when the collisional relaxation parameter v for the poloidal flow velocity is small, which corresponds to ion temperatures above a critical value. The self-generated stabilization of the fluctuation-driven transport is especially abrupt and strong. Thus the coupled turbulent transport and poloidal flow model presented here for the onset of a reduced trans-

port regime gives a useful paradigm for the experimentally observed rapid L–H transition. The experimental correlation of the transport reduction based on this Reynolds stress mechanism remains an interesting problem. In this work, only the single-helicity resistive g-mode case is examined. As a future task, we need to investigate the shear flow generation by the Reynolds stress in the case of multihelicity turbulence and other types of modes such as the ion pressure gradient-driven drift wave turbulence.

We are presently developing a simple dynamical model of the L–H transition consisting of the ordinary time-differential equations for the three variables in Eqs. (33)–(35), i.e., the shear flow kinetic energy, fluctuation kinetic energy, and the plasma internal energy, which can self-consistently describe the transport reduction, the shear flow generation, as well as the background responses, such as the changes in the pressure gradient and the damping parameter v. The reduced dynamical model uses closure relations for the two anomalous fluxes contained on the right-hand side of Eqs. (33)–(35), based on the simulations presented here. These new results will be presented elsewhere.

[1]H. Biglari, P. H. Diamond, and P. W. Terry, Phys. Fluids B **2**, 1 (1990).
[2]K. C. Shaing and E. C. Crume, Jr., Phys. Rev. Lett. **63**, 2369 (1989).
[3]S.-I. Itoh and K. Itoh, Phys. Rev. Lett. **60**, 2276 (1988).
[4]B. A. Carreras and V. E. Lynch, Phys. Fluids B **3**, 1438 (1991).
[5]P. H. Diamond and Y.-B. Kim, Phys. Fluids B **3**, 1626 (1991).
[6]J. F. Drake, J. M. Finn, P. Guzdar, V. Shapiro, V. Shevchenko, F. Waelbroeck, A. B. Hassam, C. S. Liu, and R. Sagdeev, Phys. Fluids B **4**, 488 (1992).
[7]H. Sugama and M. Wakatani, Phys. Fluids B **3**, 1110 (1991).
[8]S. Hamaguchi and W. Horton, Phys. Fluids B **4**, 319 (1992).
[9]B. A. Carreras, V. E. Lynch, L. Garcia, and P. H. Diamond, Phys. Fluids B **5**, 1491 (1993).
[10]B. A. Carreras, V. E. Lynch, and L. Garcia, Phys. Fluids B **5**, 1795 (1993).
[11]H. P. Furth, J. Killeen, and M. N. Rosenbluth, Phys. Fluids **6**, 459 (1963).
[12]B. A. Carreras, L. Garcia, and P. H. Diamond, Phys. Fluids **30**, 1388 (1987).
[13]H. Sugama and M. Wakatani, J. Phys. Soc. Jpn. **57**, 2010 (1988).
[14]W. Horton, T. Tajima, and T. Kamimura, Phys. Fluids **30**, 3485 (1987).
[15]T. Chiueh, P. W. Terry, P. H. Diamond, and J. E. Sedlak, Phys. Fluids **29**, 2341 (1986).
[16]H. R. Strauss, Plasma Phys. **22**, 733 (1980).
[17]See AIP Document No. PAPS PHPAE-01-345-50 for 50 pages of "Shear flow generation from the interaction of neoclassical and drift wave transport processes," by X. Su, P. N. Yushmanov, J. Dong, and W. Horton, IFS Report No. 617. Order by PAPS number and journal reference from American Institute of Physics, Physics Auxiliary Publi-

354   Phys. Plasmas, Vol. 1, No. 2, February 1994

H. Sugama and W. Horton

cation Service, 500 Sunnyside Boulevard, Woodbury, New York 10017-2999. The price is $1.50 for each microfiche (60 pages) or $5.00 for photocopies of up to 30 pages, and $0.15 for each additional page over 30 pages. Airmail additional. Make checks payable to the American Institute of Physics.

[18] A. B. Hassam and R. M. Kulsrud, Phys. Fluids **21**, 2271 (1978).

[19] S. P. Hirshman and D. J. Sigmar, Phys. Fluids **20**, 518 (1977).

[20] S. Hamaguchi, Phys. Fluids B **1**, 1416 (1989).

[21] N. Nakajima, Phys. Fluids B **2**, 1170 (1990).

[22] H. Sugama, N. Nakajima, and M. Wakatani, Phys. Fluids B **3**, 3290 (1991).